The Astrophysical Journal, 843:135 (10pp), 2017 July 10 https://doi.org/10.3847/1538-4357/aa755b

Galaxy-scale Bars in Late-type Sloan Digital Sky Survey Galaxies Do Not Influence the Average Accretion Rates of Supermassive Black Holes

A. D. Goulding[1], E. Matthaey[1], J. E. Greene[1], R. C. Hickox[2], D. M. Alexander[3], W. R. Forman[4], C. Jones[4], B. D. Lehmer[5], S. Griffis[2,6], S. Kanek[2], and M. Oulmakki[2]
[1] Department of Astrophysical Sciences, Princeton University, Ivy Lane, Princeton, NJ 08544, USA; goulding@astro.princeton.edu
[2] Department of Physics and Astronomy, Dartmouth College, 6127 Wilder Laboratory, Hanover, NH 03755, USA
[3] Center for Extragalactic Astronomy, Department of Physics, University of Durham, South Road, Durham DH1 3LE, UK
[4] Harvard-Smithsonian Center for Astrophysics, 60 Garden Street, Cambridge, MA 02138, USA
[5] Department of Physics, University of Arkansas, 226 Physics Building, 825 West Dickson Street, Fayetteville, AR 72701, USA
[6] Department of Computer Science, Harvard University, 33 Oxford Street, Cambridge, MA 02138, USA
Received 2016 November 18; revised 2017 May 19; accepted 2017 May 24; published 2017 July 13

Abstract

Galaxy-scale bars are expected to provide an effective means for driving material toward the central region in spiral galaxies, and possibly feeding supermassive black holes (BHs). Here we present a statistically complete study of the effect of bars on average BH accretion. From a well-selected sample of 50,794 spiral galaxies (with $M_* \sim 0.2$–$30 \times 10^{10}\,M_\odot$) extracted from the Sloan Digital Sky Survey Galaxy Zoo 2 project, we separate those sources considered to contain galaxy-scale bars from those that do not. Using archival data taken by the *Chandra* X-ray Observatory, we identify X-ray luminous ($L_X \gtrsim 10^{41}$ erg s^{-1}) active galactic nuclei and perform an X-ray stacking analysis on the remaining X-ray undetected sources. Through X-ray stacking, we derive a time-averaged look at accretion for galaxies at fixed stellar mass and star-formation rate, finding that the average nuclear accretion rates of galaxies with bar structures are fully consistent with those lacking bars ($\dot{M}_{\rm acc} \approx 3 \times 10^{-5}\,M_\odot$ yr^{-1}). Hence, we robustly conclude that large-scale bars have little or no effect on the average growth of BHs in nearby ($z < 0.15$) galaxies over gigayear timescales.

Key words: galaxies: active – X-rays: galaxies

1. Introduction

The seminal discovery that the masses of supermassive black holes (BHs) show a proportional relationship with their stellar spheroids (e.g., Magorrian et al. 1998; Ferrarese & Merritt 2000; Gebhardt et al. 2000) implies a strong physical association between the growth of BHs and the evolution of their host galaxies (e.g., Croton et al. 2006; Hopkins et al. 2006). With the advent of wide-field extragalactic surveys, we now have a panchromatic view of millions of galaxies and active galactic nuclei (AGNs). Indeed, studies performed using data from these multiwavelength surveys have revolutionized our understanding of galaxy formation, and the connections between galaxies and their central BHs (e.g., Daddi et al. 2007; Hickox et al. 2009; Donley et al. 2012; Juneau et al. 2013; Goulding et al. 2014; Jones et al. 2016; for a review, see Alexander & Hickox 2012).

The evolution of luminous AGN activity ($L_X \gtrsim 10^{44}$ erg s^{-1}) has now been traced to $z \approx 5$ (e.g., Alexander et al. 2003; Ueda et al. 2003; Hasinger et al. 2005; Mortlock et al. 2011; Xue et al. 2011; Vito et al. 2013, 2014; Aird et al. 2015; Brandt & Alexander 2015; Georgakakis et al. 2015; Marchesi et al. 2016; Vito et al. 2016). These deep and wide-field studies have revealed that galaxies undergoing a rapid stage of evolution are often found to host powerful and extremely luminous AGNs. Such luminous AGN activity is frequently associated with recent galaxy–galaxy interactions (Cisternas et al. 2011; Ellison et al. 2011; Silverman et al. 2011; Treister et al. 2012; Glikman et al. 2015; Hong et al. 2015). Though still an active area of discussion, the majority of more moderate-luminosity AGNs ($L_X \sim 10^{42} - 10^{44}$ erg s^{-1}) at $z \sim 0.1$–2 appear to be hosted in disk-like systems, that do not appear to have recently undergone a significant merger (e.g., Schawinski et al. 2011; Kocevski et al. 2012; Simmons et al. 2012; Rosario et al. 2013; Cisternas et al. 2015; Cheung et al. 2015). Hence, the evolution of these galaxies is relatively slow and largely decoupled from the cosmic framework; in turn, they must be growing their BHs through more secular processes (see below; Hopkins & Hernquist 2006; Schawinski et al. 2012).

While gas-rich mergers can readily provide a plentiful supply of material to accrete onto a BH, the dominant mechanism through which BHs grow in secularly evolving (e.g., Kormendy & Kennicutt 2004) spiral galaxies is still poorly understood. Secular evolution is expected to be primarily driven through large-scale instabilities, such as dynamic bars (e.g., Shlosman & Noguchi 1993; Courteau et al. 1996; Bournaud & Combes 2002; Sheth et al. 2005; Cheung et al. 2013; Sánchez-Janssen & Gadotti 2013; Sellwood 2014), which may have been induced by an early merger (Noguchi 1987). Through angular momentum exchange, bars generate radial flows that are capable of transporting kiloparsec-scale gas down to approximately parsec scales, close to the galaxy center (e.g., Shlosman et al. 1989; Friedli & Benz 1993; Wang et al. 2012; Fanali et al. 2015). The resulting cool gas reservoir may serve to feed the BH, and hence, bars are proposed as viable mechanisms to trigger AGN activity in spiral galaxies (e.g., Shlosman et al. 1990; Wada & Habe 1995; Bournaud & Combes 2002; Athanassoula 2003; Laurikainen et al. 2004; Jogee 2006).

However, to date, no definitive connection has been made between large-scale bar structures in spiral galaxies and the presence of a central moderate-luminosity AGN. Previous studies have primarily focused on searching for an enhancement in the bar fraction of AGNs, typically indentified through

optical emission line diagnostics, over control samples of spiral galaxies within focused high-quality nearby and large format statistical studies in the optical and near-infrared regimes, often with seemingly contradictory results (for a recent review of these results, see Table 1 of Galloway et al. 2015). More indirectly, there has also been speculation that barred spirals are offset (by a factor ∼2) from the standard BH–bulge relation (Graham & Li 2009; Brown et al. 2013); though others have found little difference between barred and non-barred systems (e.g., Xiao et al. 2011).

Previous studies have often been hampered by small number statistics. However, Galloway et al. (2015) recently harnessed the enormous wealth of morphological information available in the second release of the Sloan Digital Sky Survey citizen science project, Galaxy Zoo, to find that, at fixed stellar mass and rest-frame u–r color, galaxies hosting AGNs show a ∼16% increase in their bar fraction. Seemingly contradictory results arise from the citizen science project "Galaxy Zoo: Hubble" (Cheung et al. 2015), finding no evidence for bar enhancement in AGNs. It is therefore unclear whether a bar is the dominant factor for growing a BH in the absence of a recent merger.

A possible scenario that could explain the existence of AGNs in only some barred galaxies is that AGN activity is a stochastic process. Simulations find that the physical processes that feed BH growth on small spatial scales are unlikely to be smooth or continuous, leading BH accretion to vary dramatically on short (megayear) timescales (Hopkins & Quataert 2010; Hickox et al. 2014). This variation may hide a strong underlying correlation with longer-lived galaxy properties, such as star formation (e.g., Gabor & Bournaud 2013; Hickox et al. 2014; Thacker et al. 2014; Delvecchio et al. 2015) or the existence of a large-scale bar, which can remain in situ for significant fractions of a gigayear. A statistically complete study focused on assessing average AGN activity as a function of bar properties (rather than assessing bars in AGN hosts), and hence, a time-averaged look at BH accretion, may serve to alleviate current tensions in the literature.

X-ray observations provide a robust detection of AGN activity that is less affected by obscuration than optical light. However, through the use of "X-ray stacking techniques," these observations may also provide aggregate measurements of BH accretion rate for suitably selected galaxy samples. In relatively small (<10 deg^2) contiguous fields, X-ray stacking has been used effectively to search for faint X-ray signals of heavily obscured or low-luminosity accretion (e.g., Brandt et al. 2001; Hickox et al. 2007; Vito et al. 2016). Indeed, when combining the unprecedented angular resolution of the *Chandra* X-ray Observatory with complementary multiwavelength data, a number of studies have revealed significant populations of formally undetected AGNs (e.g., Daddi et al. 2007; Fiore et al. 2008; Georgakakis et al. 2008; Alexander et al. 2011; Chen et al. 2013), as well as the average AGN space densities and luminosity functions across cosmic time (e.g., Worsley et al. 2005; Hickox & Markevitch 2006; Xue et al. 2011). Most recently, in the COSMOS field, X-ray stacking has been used, in conjunction with the *Hubble* Space Telescope, as a first step toward addressing the question of the effectiveness of large-scale bars in driving the growth of BHs in the absence of a major merger (Cisternas et al. 2015). Based on their X-ray stacking of barred versus non-barred galaxies, Cisternas et al. (2015) find that at $z \sim 0.3$–0.8 the average AGN luminosity is not influenced by the presence of a bar.

Building on these previous studies, here we combine the unprecendented wealth of morphological information available from the Sloan Digital Sky Survey with the inherent statistical power of an X-ray stacking analysis performed using data from the *Chandra* X-ray Observatory to measure the average BH accretion rates of galaxies that do and do not contain large-scale bars. In Section 2, we describe the selection process for samples of barred and non-barred galaxies extracted from the Sloan Digital Sky Survey and Galaxy Zoo, as well as our X-ray data and stacking analyses. In Section 3, we ascertain the effect of bars on the growth of BHs in nearby galaxies, finding no difference in the average accretion rate of AGNs determined from X-ray stacking in barred galaxies compared with control samples of non-barred systems. In Section 4, we discuss the implications of our findings and present our concluding remarks. Throughout this manuscript, we adopt a flat ΛCDM cosmology with $H_0 = 71$ km s^{-1} Mpc^{-1} and $\Omega_M = 0.3$.

2. Sample Selection

In this section, we describe the selection of our uniform and optical-property matched nearby spiral galaxy sample. The source sample is selected from the ∼120 deg^2 overlap region between the Sloan Digital Sky Survey and serendipitous observations performed up to and including Cycle 16 with the Advanced CCD Imaging Spectrometer (ACIS) on board the *Chandra* X-ray Observatory. Additionally, we outline our X-ray stacking methodology used to measure the average X-ray luminosities of this galaxy sample.

2.1. Barred Galaxies in SDSS Galaxy Zoo 2

We begin by constructing a parent sample of spiral galaxies from which to select our sub-samples of galaxies with and without large-scale bars. Our sample of local galaxies is selected from the seventh data release of the Sloan Digital Sky Survey (hereafter, SDSS-DR7; Abazajian et al. 2009), where we select all spectroscopically targeted $r < 17.77$ magnitude galaxies in the redshift range of $z \sim 0.01$–0.17. Following Galloway et al. (2015), the lower redshift limit excludes those galaxies whose angular size significantly exceeds the size of the spectroscopic fiber.

Morphological cuts on the SDSS parent sample are made using visual-classification data gathered from the citizen science project, Galaxy Zoo (Lintott et al. 2008, 2011). Specifically, we harness the second release of the Galaxy Zoo project (hereafter, SDSS-GZ2) that provides detailed morphological statistics on ∼300,000 SDSS galaxies, including inclination angle, existence of spiral arms, bulge dominance, and galactic bars. These statistics are a collation of the responses to a set of hierarchical decision-tree questions, posed to citizen scientists, regarding morphological features that may or may not be present in 3-color images of SDSS galaxies (for details see Willett et al. 2013).

We identified a sample of disk galaxies by selecting all systems in SDSS-GZ2 at $0.01 \lesssim z \lesssim 0.17$ that had been visually classified by at least 20 people (i.e., the galaxy had at least 20 responses to the zeroth node question: "Is the galaxy simply smooth and rounded, with no sign of a disk?"), and where the fraction of classifiers identifying disk features (i.e., positive responses to the zeroth node question) was $f_{\rm disk} \geqslant 0.227$. Large-scale bars may be difficult to identify in objects that are highly inclined, hence, we remove likely

edge-on systems with the classification fraction threshold $f^{\rm not}_{\rm Edge\text{-}on} > 0.5$. Selecting against edge-on systems will further remove systematic bias against obscured AGNs where the AGN emission is being extinguished by line-of-sight material residing in the host galaxy (e.g., Goulding & Alexander 2009; Lagos et al. 2011; Goulding et al. 2012a), and not necessarily a small-scale dust/gas-rich torus. Performing our stacking analyses at X-ray energies will then allow us to mitigate the effects of the small-scale obscurer. Our chosen cuts on the SDSS-GZ2 are similar to those suggested by Willett et al. (2013) from their in-depth analysis of the entire SDSS-GZ2 data and catalog. After our zeroth order morphological cuts, the SDSS-GZ2 sample contains a robust sample of 96,767 spiral galaxies.

X-ray emission produced due to AGN activity and/or star-forming processes is known to be a function of galaxy stellar mass (e.g., Lehmer et al. 2010, 2016). Hence, to avoid bias and incompleteness, we require our sample to be complete in stellar mass in a given redshift bin. Due to the $r < 17.77$ mag selection, the SDSS spectroscopic galaxy sample forms a stellar mass complete sample (Brinchmann et al. 2004). At the low-redshift limit of the survey, SDSS-DR7 is complete to $M_* \sim 10^8\,M_\odot$, and allows volume-limited galaxy samples that are mass complete to be constructed to $z < 0.22$. To obtain estimates of the stellar mass and star-formation rates (SFR) for the 96,767 spiral galaxies in our SDSS-GZ2 sample, we use the value-added MPA-JHU spectroscopic catalog of Brinchmann et al. (2004). Brinchmann et al. (2004) used the SDSS `cmodel` photometry and fiber spectroscopy to fit stellar population synthesis templates using a Bayesian methodology to derive the physical properties. Here we use the 50th percentile of the log total stellar mass PDF (i.e., the median estimates of the total stellar masses), the SFR within the fiber, and the scaled total SFR. Median uncertainties are 0.09 dex and 0.14 dex on M_* and SFR, respectively.

In Figure 1, we show the distribution of the $\sim 10^5$ SDSS-GZ2 spirals with stellar mass estimates in the MPA-JHU catalog. We identify three redshift bins, 0.01–0.05, 0.05–0.09, and 0.09–0.13, where our spiral sample is complete to a given stellar mass threshold (green dashed boxes in Figure 1). These three M_*–z sub-samples form the basis for our X-ray analyses presented in Section 2.2.

We distinguish between galaxies with and without bars using the debiased fraction of votes[7] measured from the SDSS-GZ2 question: "Is there a sign of a bar feature through the center of the galaxy?" (hereafter, $f_{\rm bar}$). We select only spiral galaxies in our M_*–z samples where the number of votes on the "bar question" was $\geqslant$5. The average number of "bar question" votes per galaxy for the sample is 13. A naive cut of $f_{\rm bar} > 0.5$ provides a bar fraction of only $\sim$18%. This bar fraction is substantially below the known fraction of local ($D < 40$ Mpc) galaxies that contain a bar signature ($\gtrsim$59%) based on near-IR identification, which is far less susceptible to dust obscuration effects than optical identifications (Eskridge et al. 2000; Menéndez-Delmestre et al. 2007).

Furthermore, a simple analysis of the distribution of $f_{\rm bar}$ for SDSS-GZ2 spiral galaxies, shows it to be roughly exponentially peaked at $f_{\rm bar} \sim 0.0$ with a declining tail toward

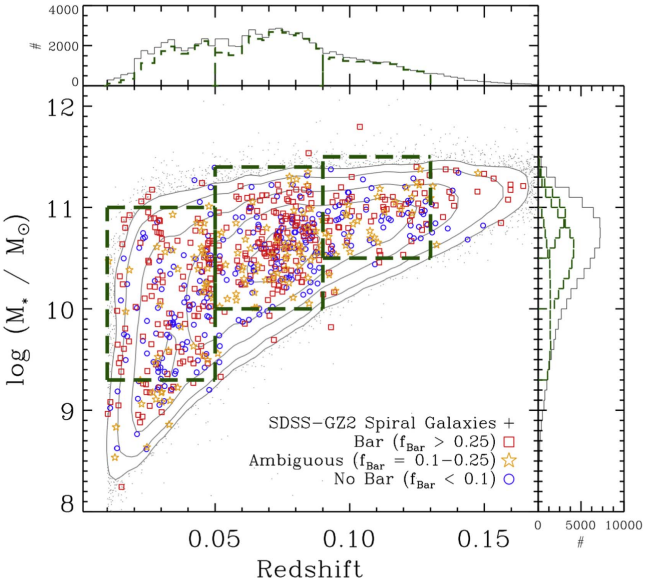

Figure 1. Main panel: stellar mass vs. spectroscopic redshift for non-edge-on ($f^{\rm not}_{\rm Edge-on} > 0.5$) SDSS-GZ2 disk galaxies (gray contours). Based on the debiased vote fraction, galaxies in the SDSS-GZ2 and *Chandra* X-ray ACIS overlap region that are determined to have bar structures ($f_{\rm bar} > 0.25$), to have no discernable bar ($f_{\rm bar} < 0.1$), and those galaxies with ambiguous evidence for a bar ($f_{\rm bar} = 0.1$–0.25) are shown with red squares, blue circles, and yellow stars, respectively. Bounding regions for three selected $M_* - z$ bins used throughout Section 3 are shown with green dashed lines. Upper panel: redshift distributions for the full SDSS-GZ2 sample (gray) and the galaxies selected in the dashed boxes in the main panel (green dashed). Right panel: stellar mass distributions for the full SDSS-GZ2 sample (gray), and the three $M_* - z$-dependent selections shown in the main panel (green dashed).

$f_{\rm bar} \sim 1.0$. The shape of this distribution is likely driven by observational biases, as the true probability distribution of bar versus non-bars in spiral galaxies must be far more bi-modal. Hence, $f_{\rm bar}$ does not directly map to the probability of a bar existing in a particular spiral galaxy.

In order to separate barred galaxies from non-barred galaxies, we use the known nearby bar fraction ($\gtrsim$59%), and match this to the cumulative distribution of $f_{\rm bar}$ for the SDSS-GZ2 parent spiral sample. A demarcation of $f_{\rm bar} \gtrsim 0.15$ results in a bar fraction of $\sim$55%. Given small number statistics, and allowing for the possibility of false-positives, we conservatively use a threshold of $f_{\rm bar} \geqslant 0.25$, providing us with a "clean" bar sample (bar fraction of $\sim$40%).[8] Similarly, if we adopt a threshold of $f_{\rm bar} < 0.1$, we achieve a "clean" non-barred spiral sample with a non-bar fraction of $\sim$40%. The remaining $\sim$20% of galaxies in our M_*–z samples with $0.1 < f_{\rm bar} < 0.25$, in a purely statistical sense, have ambiguous evidence for the presence of a bar. This is further evidenced in Figure 2, where we provide example images used in GalazyZoo2 to classify the galaxies. Sources with $f_{\rm bar} \geqslant 0.25$ seemingly have strong and/or obvious bar structures, while those with $0.1 < f_{\rm bar} < 0.25$ have much weaker and/or difficult to identify bars in their SDSS 3-color images. In Table 1, we provide the number of non-edge-on spiral galaxies in our M_*–z samples determined to have bars (28,733 galaxies), no bars (28,728 galaxies), and ambiguous evidence for bars (15,474 galaxies).

[7] The desbiased fraction of votes are the fraction of votes cast by citizen scientists on a particualr classification question, which have been weighted for consistency and adjusted for redshift dependent classification bias. See Section 3.3 of Willett et al. (2013) for further details.

[8] Our bar selection threshold is also similar to a cut of $f_{\rm bar} > 0.3$ that was determined from the independent analysis of Willett et al. (2013). See also Galloway et al. (2015).

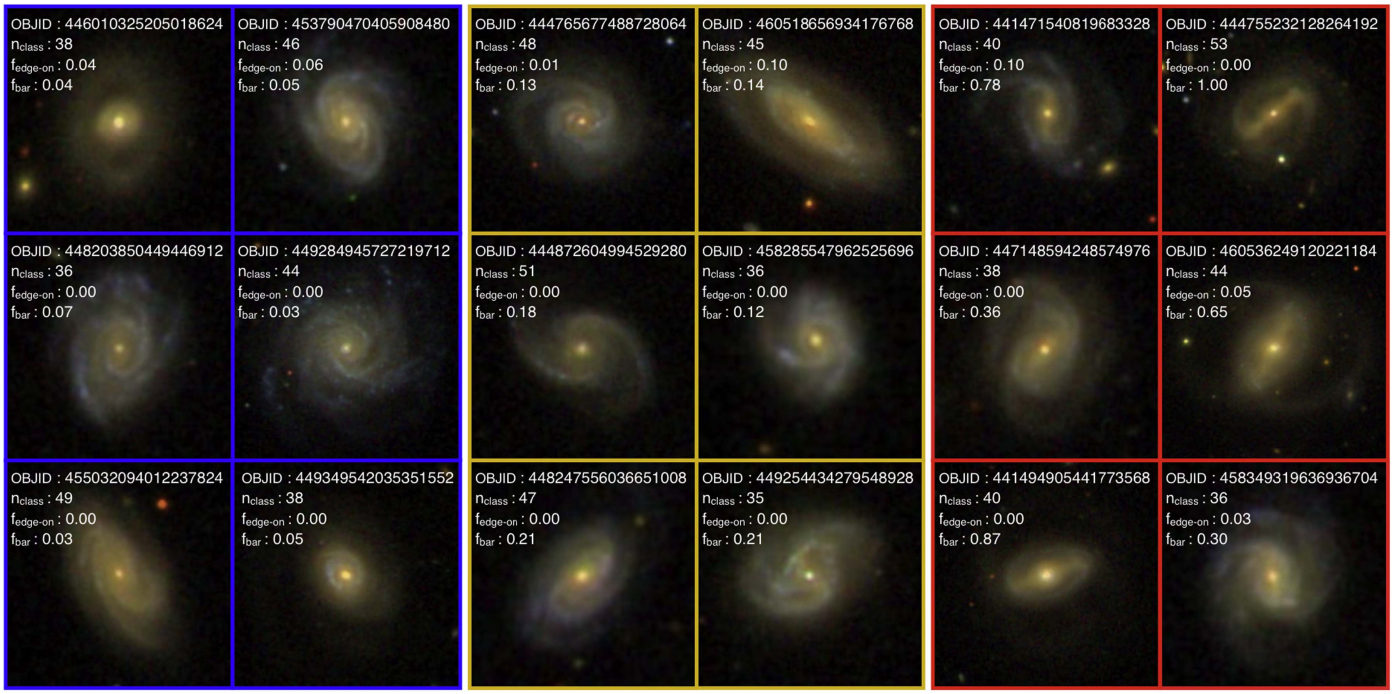

Figure 2. Three color (*gri*) composite SDSS-Legacy images for a random set of sources from the SDSS-GZ2 galaxy sample. Colored lines highlight sources with $f_{\rm bar} > 0.25$ (red), $f_{\rm bar} = 0.1$–0.25 (yellow), and $f_{\rm bar} < 0.1$ (blue). Individual galaxies are labeled with their SDSS unique object identifier number (objid), the number of citizen scientists who classified the galaxy ($n_{\rm class}$), the edge-on debiased vote fraction ($f_{\rm edge-on} = 1 - f^{\rm not}_{\rm edge-on}$), and the galaxy-bar present debiased vote fraction ($f_{\rm bar}$).

Finally, to statistically compare the AGN properties of our M_*–z samples based on their inferred bar properties, it is important to ensure that the distributions of the first-order galaxy properties (such as SFR; stellar mass) are well matched between the bar/no-bar sub-populations. In Figure 3, we provide the SFR measured within the spectroscopic fiber and the stellar mass distributions of the three M_*–z samples, separated based on their inferred bar properties. Based on two-sample Kolmogorov–Smirnov (K–S) tests, we find evidence at the >99.99% level that the SFR distributions for the bar and non-bar samples are not drawn from the same distributions ($P < 10^{-7}$; see also Oh et al. 2012). It is further evident from the histograms presented in Figure 3 that, as a function of M_* and z, there is an increasing fraction of barred galaxies with low SFRs over those without bars. It is beyond the scope of this study to provide a full explanation for this phenomenon, though we suggest that it may be easier to visually identify bars in systems that lack significant levels of SF or that star-forming regions may systematically reside at larger radii in barred galaxies (Robichaud et al. 2017).

For the purposes of our experiment, it is sufficient to simply ensure that the distributions in galaxy properties are similar for the barred and non-barred stacked samples. Hence, to mitigate these effects, we apply SFR cuts of $\log {\rm SFR}/(M_\odot\ {\rm yr}^{-1}) > -1.8$, >-1.4, and >-1.0 for our M_*–z redshift bins of 0.01–0.05, 0.05–0.09, and 0.09–0.13, respectively. We find that these cuts are sufficient to simultaneously remove the tensions between the SFR and M_* distributions for the SDSS-GZ2 galaxies included in our X-ray stacking analysis (described in the next section). Comparing the SFR distributions for the barred and non-barred that are covered by *Chandra* X-ray observations, from two-sample K–S tests we find $P \gtrsim 0.2$ between the $0.01 < z < 0.05$ and $0.05 < z < 0.09$ samples, while we still find some evidence for tension ($P \sim 0.015$) between the samples at $0.09 < z < 0.13$.

While not fully essential for our analyses because we also take care to statistically account for X-ray emission from SF in our stacking analysis, requiring similar distributions in M_* and SFR is still a useful endeavor when comparing the X-ray properties of galaxies as it equally aggregates the contamination to the X-ray emission from SF processes, while also allowing us to (statistically) select sources hosting similar mass BHs (through the M_*–$M_{\rm BH}$ correlation).

2.2. STACKFAST: X-Ray Stacking Analyses

Stacking analyses are based on the principle that objects at known positions, which are not detected individually in imaging at a particular wavelength, may show a significant flux when the observations are averaged together. These aggregate measurements are most accurate when both the multiwavelength properties of the stacked sample are previously well defined and source number statistics are sufficiently high to break through the noise floor, and thus, increase the signal-to-noise and effective depth of the observations. By definition, these stacked signals then have the added effect of averaging over the inherent stochasticity of AGN accretion, which is present in blind selections of AGN samples.

To perform the X-ray stacking of our sample, we used our custom IDL-based software STACKFAST, which is designed specifically for *Chandra* ACIS data and we briefly describe here (see also Hickox & Markevitch 2007; Hickox et al. 2007, 2009; Chen et al. 2013). STACKFAST begins with two elements: a master catalog of input sources, and a set of uniformly formatted, reduced, and flare-cleaned *Chandra* ACIS data products derived from individual *Chandra*-ACIS observations

Table 1
Galaxy Sample and X-Ray Stacking Results

						0.5–2 keV				2–7 keV				0.5–7 keV			
$\log M_*$	z	$f_{\rm bar}$	# SDSS	$\bar{t}_{\rm Exp}$	$\Sigma t_{\rm Exp}$	# Det.	# Stack	$\bar{L}_{\rm X,AGN}$ 10^{39}	S/N	# Det.	# Stack	$\bar{L}_{\rm X,AGN}$ 10^{39}	S/N	# Det.	# Stack	$\bar{L}_{\rm X,AGN}$ 10^{39}	S/N
($M_\odot$)				(ks)	(ks)			(erg s^{-1})				(erg s^{-1})				(erg s^{-1})	
(1)	(2)	(3)	(4)	(5)	(6)	(7)	(8)	(9)	(10)	(11)	(12)	(13)	(14)	(15)	(16)	(17)	(18)
9.3–11.0	0.01–0.05	>0.25	5958	33.8	2905.8	17	63	$1.56^{+0.42}_{-0.43}$	10.7	13	67	$2.88^{+0.67}_{-0.65}$	8.2	18	62	$3.47^{+0.97}_{-1.04}$	13.5
		0.1–0.25	3486	24.5	770.0	10	21	$1.02^{+0.76}_{-0.62}$	5.4	10	21	$1.11^{+1.31}_{-0.90}$	3.3	10	21	$0.59^{+1.70}_{-0.58}$	6.3
		<0.1	6543	24.7	1444.3	17	57	$1.01^{+0.68}_{-0.83}$	10.1	14	60	$1.63^{+0.80}_{-0.61}$	6.9	16	58	$0.48^{+2.30}_{-0.35}$	12.2
10.0–11.4	0.05–0.09	>0.25	8644	17.0	1448.5	17	60	$3.60^{+1.91}_{-1.65}$	7.9	13	64	$5.75^{+4.00}_{-4.62}$	6.1	15	62	$7.66^{+4.79}_{-5.48}$	10.0
		0.1–0.25	5637	22.0	1035.6	8	37	$4.07^{+1.25}_{-1.23}$	7.1	7	38	$1.31^{+3.79}_{-2.82}$	3.8	8	37	$5.33^{+3.45}_{-2.31}$	8.0
		<0.1	10059	22.1	1552.2	13	54	$2.87^{+1.17}_{-1.04}$	6.9	12	55	$3.39^{+3.06}_{-2.70}$	5.0	13	54	$5.04^{+3.22}_{-2.68}$	8.5
10.5–11.5	0.09–0.13	>0.25	4074	27.3	1090.4	8	27	$8.20^{+3.76}_{-2.78}$	6.3	6	29	$19.2^{+7.81}_{-5.81}$	5.5	8	27	$22.1^{+10.7}_{-7.59}$	8.3
		0.1–0.25	2401	35.9	970.8	3	19	$3.19^{+2.48}_{-1.98}$	4.7	2	20	$13.2^{+6.18}_{-5.00}$	5.1	3	19	$11.3^{+6.51}_{-5.50}$	7.0
		<0.1	3992	33.5	1272.8	7	29	$4.16^{+1.89}_{-1.77}$	4.6	3	33	$17.2^{+10.5}_{-12.8}$	5.3	6	30	$1.43^{+7.41}_{-8.70}$	7.1

Note. (1) Ranges of the logarithm of the stellar mass in units of solar masses; (2) redshift ranges; (3) fraction of citizen scientists voting for the presence of a bar in the SDSS image; (4) number of SDSS-GZ2 galaxies in each bin matched for similar distributions in star-formation rates measured within the SDSS spectroscopic fiber; (5) mean exposure time of all galaxies covered by *Chandra* ACIS-I observations in units of kiloseconds; (6) total exposure time for all galaxies covered by *Chandra* ACIS-I observations in units of kiloseconds; (7–10) number of X-ray detected AGNs in the 0.5–2 keV band, number of non-X-ray detected galaxies included in the X-ray stack, star-formation-subtracted stacked (average) X-ray luminosity (in units of 10^{39} erg s^{-1}) in the 0.5–2 keV band, signal-to-noise of the X-ray emission in the stack above the stacked local background; (11–14) same as columns 7–9 in the 2–7 keV band; (14–18) same as columns 7–9 in the 0.5–7 keV band.

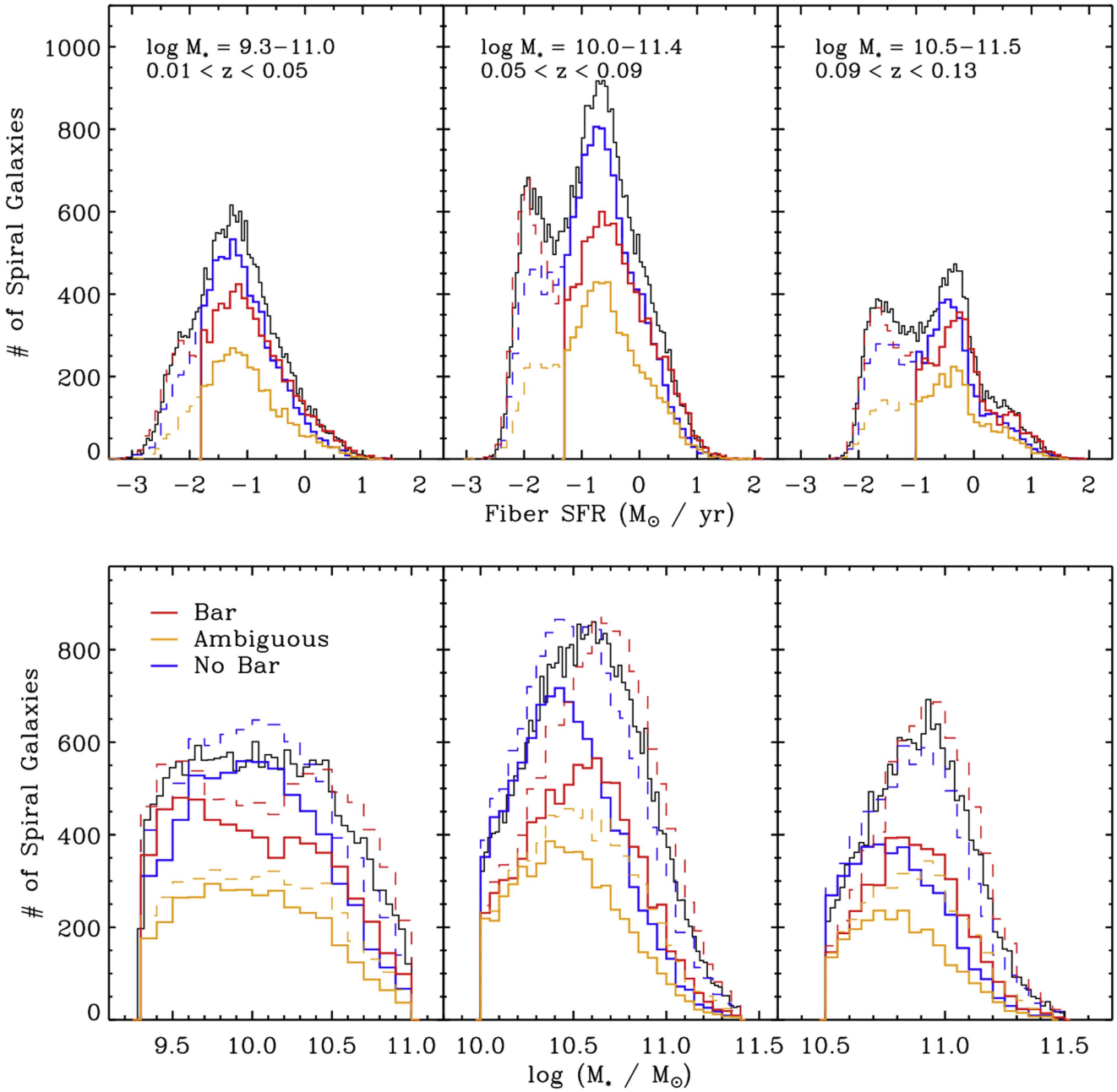

Figure 3. Upper panel: histograms of star-formation rates within the SDSS spectroscopic fiber for all SDSS-GZ2 galaxies in the $M_* - z$ bins (black solid lines) shown in Figure 1. Lower panel: histograms of total stellar mass. Common: colored lines represent SDSS-GZ2 galaxies with $f_{\rm bar} > 0.25$ (red), $f_{\rm bar} = 0.1$–0.25 (yellow), and $f_{\rm bar} < 0.1$ (blue). Dashed lines represent the full galaxy samples in their respective bar category. Solid lines represent the galaxies used throughout our analyses in Section 3 after matching the samples on star-formation rate.

(ObsIDs). Here we include all ACIS ObsIDs that were publicly available from Cycles 1–16 of the *Chandra* mission. ObsIDs were reduced using version 4.6 of the CIAO software package and by applying v4.6.5 of the CALDB calibration files. Events were screened using the grade set 0, 2, 3, 4, 6, and 3σ background flares were removed using the `lc_clean` tool. Aspect histograms were constructed using the `aspecthist` tool available in the CHAV software package, and convolved with the ACIS chip-map to generate observation exposure maps. For a detailed explanation of the reduction and processing procedure, see Goulding et al. (2012b).

Sources from our master catalog that lie within the field of view of an ObsID are identified, and events/photon information (position, energy, grade, and time) are extracted from a $30'' \times 30''$ box centered on the input source for each associated ObsID. STACKFAST also determines the effective exposure time at the position of the input source for each ObsID, including the effects of vignetting at large angles from the pointing axis. The result is an output file containing a stackable X-ray event list and list of exposure times for each source in the master catalog, and associated ObsID.

Once the extraction of the stackable database is performed, the next step for STACKFAST is co-adding a specific subset of sources to yield average background-subtracted X-ray count rates and fluxes in user-defined energy bands. A key consideration is the variable point-spread function (PSF) for

Chandra as a function of off-axis angle, which we characterize by the 90% energy-encircled radius[9] (r_{90}). STACKFAST extracts photons within r_{90} and assesses the background on a source-by-source basis, as variations in the PSF also affects background estimates. Local backgrounds are measured by masking high significance (`wavdetect` threshold 10^{-7}) sources that may be identified in the $30'' \times 30''$ extraction boxes, and then rescaling the photon counts, in the remaining extraction area at radii larger than $1.3 \times r_{90}$, to the source extraction area (within r_{90}). These local background measurements are co-added, and used to measure the signal-to-noise of the source stacks.

During the co-adding process, we exclude sources that lie within $5''$ of the pointing position of a particular ObsID because these sources may have been the subject of the proposed observation. The inclusion of these "proposed" sources would introduce a selection bias into the final X-ray stack. Furthermore, we also exclude input sources that are significant X-ray detections, fall on chip-gaps, or are positioned at large off-axis angles $>6'$ in a particular ObsID, as background estimation may be inaccurate or severely enhanced due to the large angular size of an X-ray point source ($\sim$5–7.″5 at E $\sim$1.5–7 keV). The final co-adding procedure is extremely efficient, and thus, readily allows bootstrap realizations to be performed to derive count rate uncertainties on the stacking measurements. In any given X-ray energy band, the final outputs from STACKFAST are average X-ray count rates within r_{90}, average X-ray backgrounds predicted within r_{90}, hardness ratios, and associated statistical uncertainties from 1000 bootstrap realizations. X-ray count rates are converted to fluxes assuming a power law with slope $\Gamma = 1.8$ and a *Chandra* ACIS-I response function from Cycle 9 (an average of the collation of observations used throughout our stacking).

Of the 50,794 spiral galaxies in the M_*–z sub-samples, 468 ($\sim$1%) of the sources are within $6'$ of the pointing position of at least one *Chandra* ACIS-I observation, and also are not on chip-gaps or close ($<5''$) to the pointing position. There are 101 galaxies that we determine to have significant (3σ) X-ray emission above the estimated local background that is close to the optical position. Each of the X-ray detected sources have centroids within 0.″9 of the optical position, with a median offset of $\delta_{X-O} \sim 0.''26$. This results in a sample of 367 X-ray undetected galaxies that are included as part of our stacking analysis in Section 3.

3. Results

To search for a connection between the average growth of supermassive BHs and the existence of a large-scale bar in spiral galaxies, we perform an X-ray stacking analysis of nearby spiral galaxies. As described in the previous section, we have selected samples of SDSS-GZ2 galaxies that are matched in stellar mass, SFR, and redshift. These are separated between barred ($f_{bar} > 0.25$), non-barred ($f_{bar} < 0.1$), and ambiguously barred ($f_{bar} = 0.1$–0.25) systems based on the fraction of votes received from citizen scientists using the SDSS imaging.

3.1. The Average Accretion rate of (un)-barred Spiral Galaxies

The majority of BHs residing at galaxy centers are in a low-Eddington state ($\lambda_{Edd} = L_{AGN}/L_{Edd} \lesssim 10^{-3}$), and thus, their subsequent AGN emission would fall substantially below the detection threshold of a typical extragalactic survey. Our primary goal is to harness the power of X-ray stacking to ascertain the average X-ray luminosity (in a given energy band) produced due to accretion onto the vast-majority of BHs, not only the BHs accreting above a substantial fraction of Eddington, and subsequently ask how this average accretion rate relates to the existence of a large-scale bar.

Using STACKFAST, we perform an X-ray stacking analysis (described in Section 2.2) on our spiral galaxy sample based on their perceived bar properties. Given the known scaling relations between the stellar content and the masses of BHs (e.g., McConnell & Ma 2013; Reines & Volonteri 2015), we statistically negate the effects of changing X-ray luminosities and Eddington ratios, due to differing BH mass distributions, by stacking our parent sample in bins complete in both stellar mass and redshift, i.e., the M_*–z sub-samples that we describe in Section 2. To also ensure that no one stack is biased in sensitivity compared to the other stacks, we used a K–S test to search for evidence of significant differences in the distribution of exposure times for the sources within the stacks. Based on the K–S statistic, we found no evidence for significant differences in the t_{exp} distributions when comparing the f_{bar} samples in a given $M_* - z$ bin. Furthermore, to prevent bias toward artifically high stacked luminosities due to significant individual detections, we do not include the X-ray bright sources, and defer their analysis to Section 3.2. In Figure 4, we present the results of the X-ray stacks performed in three energy bands (E = 0.5–2, 2–7, 0.5–7 keV) for our three M_*–z sub-samples separated in bins of f_{bar}.

Detailed *Chandra* studies of nearby star-forming and passive galaxies have shown that in the absence of AGN activity, the X-ray emission from hot diffuse gas, young high-mass X-ray binaries, and older low-mass X-ray binaries correlates with the SFR and M_*, respectively (e.g., Gilfanov 2004; Revnivtsev et al. 2007). This X-ray emission produced due to X-ray binaries ($L_{X,SF}$) is an obvious source of contamination in our total X-ray stacked luminosity ($L_{X,tot}$). We estimate and statistically remove $L_{X,SF}$ from $L_{X,tot}$ by calculating the log-mean SFR and M_* of the stacked galaxy sample and invoking the local relations of Lehmer et al. (2010) and Pereira-Santaella et al. (2011). Specifically, in the 0.5–2 keV band, we use Equation (4) presented in Pereira-Santaella et al. (2011), and in the 2–7 keV band, we use the SFR-dependent relation $\log L_X = 39.46 + 0.76\log$ SFR presented in Lehmer et al. (2010), and linearly combine both $L_{X,SF}$ predictions in the 0.5–7 keV. Both Lehmer et al. (2010) and Pereira-Santaella et al. (2011) invoke a Kroupa (2001) initial mass function to compute M_* and SFRs in their models, this is consistent with assumptions used for the SDSS M_* and SFR measurements taken from Brinchmann et al. (2004). After subtraction of the average $L_{X,SF}$ in the relevant bands, we produce clean average X-ray luminosities due to BH accretion[10] ($L_{X,AGN} = L_{X,tot} - L_{X,SF}$). We observe average X-ray luminosities of $L_{X,AGN} \sim (0.1$–$2) \times 10^{40}$ erg s^{-1} for the stacked samples. The stacks have typical S/Ns of $\sim$5–10 calculated using the stacked counts within the r_{90} region, and the predicted counts within r_{90} using stacked local backgrounds (see Section 2.2. These results are presented in Table 1 for the three energy ranges considered here.

[9] r_{90} is calculated based on ACIS-I PSF maps that are constructed at 0.5–2 keV, 2–7 keV, and 0.5–7 keV.

[10] We note that had we chosen to take the linear median of the SFRs and M_*, our average $L_{X,SF}$ estimates would be systematically lower by 0.06 dex.

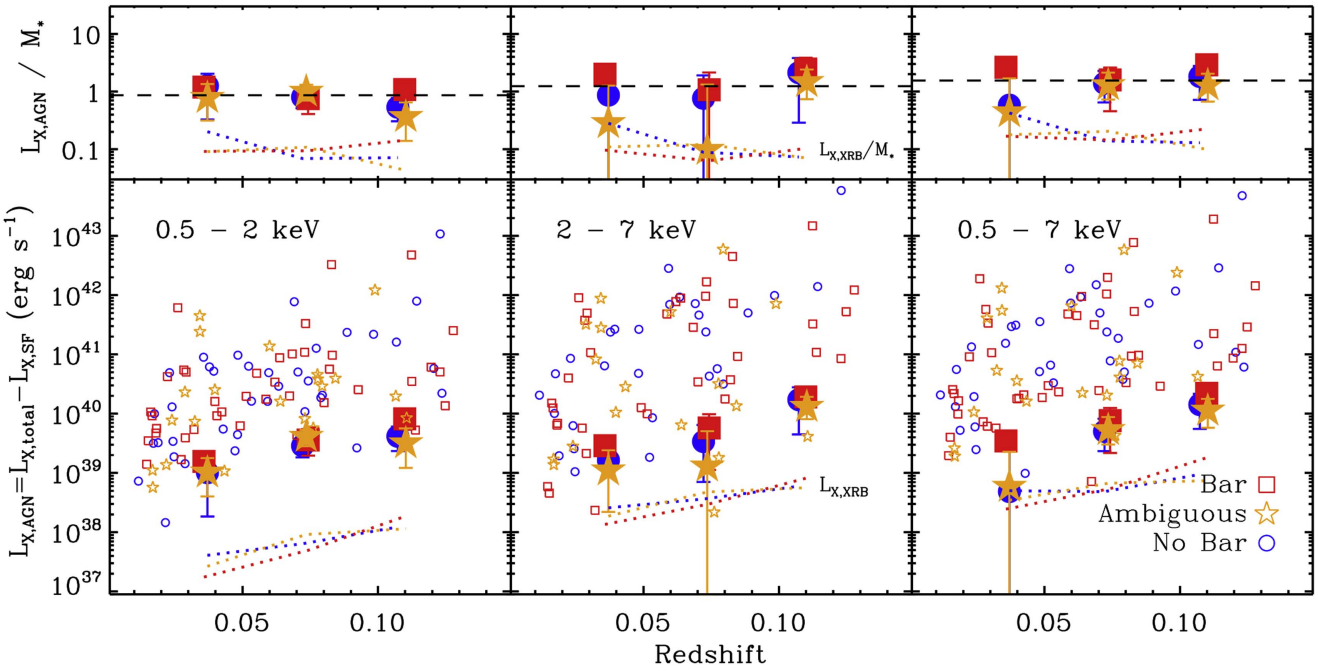

Figure 4. Lower panels: star formation subtracted AGN X-ray luminosity vs. redshift in the 0.5–2 keV (left column), 2–7 keV (center column), and 0.5–7 keV (right column) energy bands. Individual redshift bins are matched in M_* and SFR for SDSS-GZ2 galaxies in the SDSS-CXO overlap region. SDSS-GZ2 systems with $f_{bar} > 0.25$, $f_{bar} = 0.1$–0.25, and $f_{bar} < 0.1$ are shown with red squares, blue circles, and yellow stars, respectively. X-ray detected sources with S/N $\gtrsim 5$ close to the optical position are shown with open symbols, and luminosities produced from stacking of X-ray undetected sources are shown with large filled symbols. 90th percentile uncertainties on the X-ray stacks are calculated through Bootstrap resampling of the sources within the stacks. For illustration purposes, the predicted mean X-ray luminosities produced due to stellar processes are shown with dotted lines for each stacked redshift bin. Upper panels: specific AGN X-ray luminosities (i.e., $L_{X,AGN}$ normalized by median stellar mass in units of 10^{29} erg s^{-1} $M_\odot^{-1}$). The thick dashed line shows the median of the X-ray stacks. We find that there is no positive effect between the average BH accretion rate and the presence of a large-scale bar in nearby spiral galaxies, and when normalized for stellar mass this is also independent of redshift.

In Figure 4, we show that within a given redshift bin there is no significant difference (at the 90% level) between the average $L_{X,AGN}$ for barred ($f_{bar} > 0.25$), non-barred ($f_{bar} < 0.1$), and ambiguously barred ($f_{bar} = 0.1$–0.25) spiral galaxies in SDSS-GZ2. We further tested this result by selecting a sample of galaxies over the full redshift range, $0.01 < z < 0.13$, within a relatively small stellar mass range of $M_* \sim (3\text{–}10) \times 10^{10}\,M_\odot$, and performed an additional stacking analysis. This sample included 58 barred, 36 ambiguously barred, and 72 non-barred galaxies. We again found no statistical difference between the average $L_{X,AGN}$ in any of the three energy ranges. Additionally, if N_H were playing a significant role in our findings, then we would expect such a result to manifest in the hardest energy band. However, we find no significant difference between bars and non-barred galaxies in any of the three X-ray energy ranges, suggesting that our result is independent of obscuration effects.

While independent of the presence of a bar, we also find in Figure 4 a trend of increasing $L_{X,AGN}$ with z. While the f_{bar} samples within a particular redshift bin are matched in SFR and M_*, they are systematically different between the redshift bins. Galaxies at higher-z have systematically higher M_* in our sample due to the limiting magnitude of SDSS. Due to the known relation between M_* and M_{BH}, a systematically larger M_* at a given z will produce a higher average $L_{X,AGN}$ in each redshift bin.[11] We show in the upper panel of Figure 4 that when $L_{X,AGN}$ is normalized by average M_* between the redshift bins, the resultant specific accretion rate is independent of redshift in each energy range. Thus, we can robustly conclude that there is no obvious positive effect between the average X-ray luminosity associated with BH accretion and the presence of a large-scale bar in nearby spiral galaxies.

3.2. Accretion onto X-Ray Detected AGNs Residing in Barred Spiral Galaxies

As part of our stacking analysis, we used forced photometry to additionally detect (S/N $\gtrsim 5$) 101 (out of the 468 optical galaxies) X-ray point-sources that were spatially coincident (median offset of $0''.26$) with the optical nuclear position of the galaxies. While each X-ray source is presumed to be an AGN, X-ray emission from circumnuclear star formation could still contribute to the measured X-ray flux. Hence, we remove this contamination following the same procedure used in the stacks. The X-ray detected AGNs in our sample have derived luminosities of $L_{X,0.5-7keV} \sim 9 \times 10^{38}$–$5 \times 10^{43}$ erg s^{-1}, similar to X-ray luminous AGNs identified in detailed studies of local ($D \lesssim 50$ Mpc) galaxies (e.g., LaMassa et al. 2011).

We use the X-ray detected sources to further validate our stacking results found in the previous section by producing an average stack that includes both the detected and undetected X-ray sources. We exclude the 16 AGNs with $L_{X,0.5-7\,keV} > 10^{42}$ erg s^{-1}, which form the higher luminosity tail of the AGN distribution in these sources, and then stack all (X-ray detected and undetected) sources observed with sufficient depth to detect an AGN if it were to have had $L_X > 10^{42}$ erg s^{-1}. This has the added effect of removing

[11] Assuming a universal Eddington ratio distribution (e.g., Aird et al. 2012), larger average M_*, and hence, larger average M_{BH}, allows one to probe larger L_X. Higher L_X that would be otherwise prohibited due to the Eddington limit for low-mass BHs, become feasible at larger M_{BH}, i.e., the fraction of BHs capable of producing high L_X becomes larger with increasing BH mass.

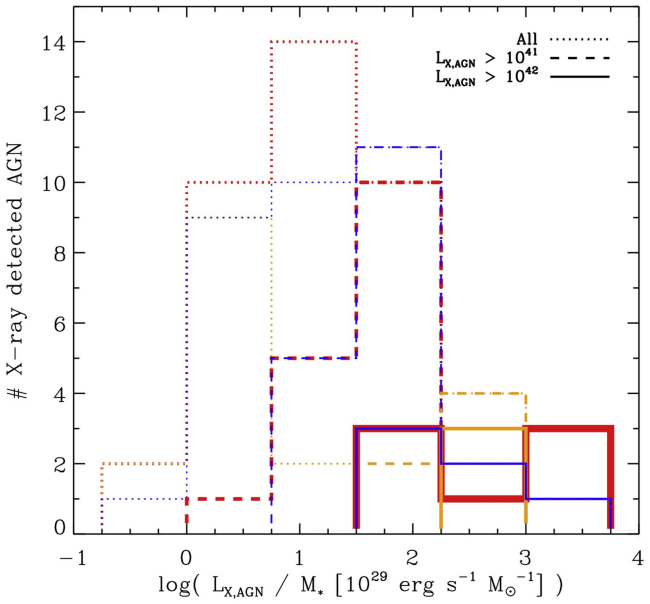

Figure 5. Specific accretion rate distributions ($L_{X,0.5-7\,keV}/M_*$) for X-ray detected galaxies in our parent mass–SFR-matched SDSS-GZ2 sample. Barred ($f_{bar} > 0.25$), ambiguous ($0.1 < f_{bar} < 0.25$), and unbarred ($f_{bar} < 0.1$) spirals are plotted with red, orange, and blue lines, respectively. Dotted, dashed, and solid lines represent the full galaxy samples, with a cut of $L_X > 10^{41}$ erg s^{-1}, and with a cut of $L_X > 10^{42}$ erg s^{-1}, respectively.

sources from the stack with extremely shallow X-ray observations. With the inclusion of the detected sources, we observed marginally higher (∼0.17–0.26 dex) $L_{X,AGN}$ in the stacked luminosities when compared to the measurements presented in Table 1. However, crucially, we still found no significant difference in the average $L_{X,AGN}$ between the f_{bar} sub-samples when including the X-ray detected sources.

We find that the detected X-ray AGN luminosities are, in general, at or above the stacked luminosities, suggesting that the stacks are measuring the peak of the luminosity distribution of the overall population, and the detected sources are populating a high-Eddington tail of the accretion rate distribution. In Figure 5, we present the specific accretion rate (L_X/M_*) distributions for the X-ray detected (at 0.5–7 keV) barred, ambiguous, and unbarred SDSS-GZ2 galaxies. Consistent with our finding of no dependence of average accretion rate on the presence of a bar, we also show that there is no difference between the specific accretion rates between barred and non-barred galaxies for the X-ray detected AGNs either (two-sample KS reveals $P \sim 0.73$).

Differences between fueling of BHs due to the presence of a bar may only become apparent when considering the most rapidly growing BHs in the sample. Hence, we further investigated whether increasing thresholds in X-ray luminosity, i.e., higher accretion rates, would produce differences in the tails of the specific accretion rate distributions for the galaxies in our sample. Applying cuts in X-ray luminosity of $L_X > 10^{41}$ erg s^{-1} and $L_X > 10^{42}$ erg s^{-1}, we find that the peak of the distributions for barred and non-barred galaxies shifts toward higher specific accretion rates. However, we show in Figure 5 that these peaks and the overall distributions remain statistically the same between the barred and non-barred systems, irrespective of the L_X cuts. There is extremely marginal evidence for an upturn at the highest specific accretion rates probed by our sample ($L_X/M_* > 10^{32}$ erg s^{-1} $M_\odot^{-1}$) for the barred galaxies, though this is within the statistical uncertainties of the sample.

Taken together, we find no statistical evidence for a difference in the specific accretion rate distributions of BHs present in barred or non-barred galaxies. Thus, even over long ∼Gyr timescales, a large-scale bar appears to have no effect on the growth of the central BH in a spiral galaxy.

4. Discussion and Conclusions

We have investigated the X-ray luminosities of a large unbiased sample of spiral galaxies selected from the SDSS-GZ2 based on the presence or absence of a large-scale bar. Based on our X-ray stacking analysis of archival *Chandra* X-ray data, we find that the average X-ray luminosities of nearby ($z < 0.15$) spiral galaxies are independent of the existence of a bar. A similar result is also seen at $z \sim 0.2$–0.8, where Cisternas et al. (2015) observed no systematic difference in the average X-ray luminosites between barred and unbarred systems assessed from *HST* morphologies in the COSMOS field. Indeed, allowing for the systematic shift to larger stellar masses in the higher redshift sample, we find consistent X-ray luminosities with the X-ray stacking analyses of Cisternas et al. (2015). Furthermore, consistent with results derived from more samples of very nearby galaxies (e.g., Ho et al. 1997; Cisternas et al. 2013), we also find no observable difference between the host galaxies of X-ray luminous AGNs on the basis of the presence of a bar.

In a given redshift bin, our stacked samples are matched in stellar mass, and hence, on average, they can be considered to also be matched in BH mass. Focusing on the $z \sim 0.05$–0.09 bin, where source numbers are largest, we can use the local M_*–M_{BH} relation (see Equations (4) and (5) of Reines & Volonteri 2015) to derive the average accretion rates ($\dot{M}_{acc}$) and λ_{Edd} for galaxies based on the presence (or absence) of a bar. The average BH mass for the sample is $\langle M_{BH} \rangle \sim 2 \times 10^7\,M_\odot$. Adopting a bolometric correction factor of $\kappa \sim 20$ (Vasudevan & Fabian 2009), and assuming an average column density for the sample of $N_H = 3 \times 10^{21}$ cm^{-2} and spectral slope $\Gamma = 1.8$, the average bolometric luminosity, independent of the presence of a bar is $L_{bol,AGN} \approx 2 \times 10^{41}$ erg s^{-1}. Further assuming a typical accretion efficiency of $\eta \sim 0.1$, this corresponds to $\dot{M}_{acc} \approx 3 \times 10^{-5}\ M_\odot$ yr^{-1} or $\lambda_{Edd} \approx 2 \times 10^{-4}$. These low average accretion rates are typical of all very nearby AGNs, when sufficiently sensitive data is available to probe these low accretion rates (e.g., Goulding et al. 2010). Hence, this suggests that, over long timescales, the presence of a bar has little effect on the growth of BHs.

In order for our and previous analyses not to detect a significant effect of a bar on the growth of the central BH, any causality between these would need to be extremely short-lived, possibly occurring only during the event that caused the bar to form (e.g., through a minor merger). Such an event could potentially provide a short-term (∼100–300 Myrs) supply of fuel for the BH, causing a rapid growth phase. However, the resultant bar structure is substantially longer lived (∼1–2 Gyrs; Bournaud et al. 2005), and will remain in situ long after the BH has exhausted any new fuel supply brought in through a minor merger. Our X-ray stacking analysis is particularly sensitive to this long-lived phase and shows that once the bar has formed, and over its lifetime, there is no substantial net positive effect on the growth of the BH.

We thank the anonymous referee for their careful reading and insightful comments that significantly improved the manuscript. A.D.G. acknowledges support for this research from the National Aeronautics and Space Administration through *Chandra* Award Number AR3-14016A issued by the *Chandra* X-ray Observatory Center, which is operated by the Smithsonian Astrophysical Observatory for and on behalf of the National Aeronautics Space Administration under contract NAS8-03060. D.M.A. thanks the Science and Technology Facilities Council (STFC) for support through grant ST/L00075X/1. R.C.H. acknowledges support from the National Science Foundation through CAREER award 1554584, and from NASA grant number NNX15AU32H. The scientific results reported in this article are based on data obtained from the *Chandra* Data Archive. This research has made use of software provided by the *Chandra* X-ray Center (CXC) in the application packages CIAO, ChIPS, and Sherpa. This research also made use of the SDSS-III database. Funding for SDSS-III has been provided by the Alfred P Sloan Foundation, the Participating Institutions, the National Science Foundation, and the U.S. Department of Energy Office of Science.

Facility: Chandra (ACIS).

References

Abazajian, K. N., Adelman-McCarthy, J. K., Agüeros, M. A., et al. 2009, ApJS, 182, 543
Aird, J., Alexander, D. M., Ballantyne, D. R., et al. 2015, ApJ, 815, 66
Aird, J., Coil, A. L., Moustakas, J., et al. 2012, ApJ, 746, 90
Alexander, D. M., Bauer, F. E., Brandt, W. N., et al. 2003, AJ, 126, 539
Alexander, D. M., Bauer, F. E., Brandt, W. N., et al. 2011, ApJ, 738, 44
Alexander, D. M., & Hickox, R. C. 2012, NewAR, 56, 93
Athanassoula, E. 2003, MNRAS, 341, 1179
Bournaud, F., & Combes, F. 2002, A&A, 392, 83
Bournaud, F., Combes, F., & Semelin, B. 2005, MNRAS, 364, L18
Brandt, W. N., & Alexander, D. M. 2015, A&ARv, 23, 1
Brandt, W. N., Alexander, D. M., Hornschemeier, A. E., et al. 2001, AJ, 122, 2810
Brinchmann, J., Charlot, S., White, S. D. M., et al. 2004, MNRAS, 351, 1151
Brown, J. S., Valluri, M., Shen, J., & Debattista, V. P. 2013, ApJ, 778, 151
Chen, C.-T. J., Hickox, R. C., Alberts, S., et al. 2013, ApJ, 773, 3
Cheung, E., Athanassoula, E., Masters, K. L., et al. 2013, ApJ, 779, 162
Cheung, E., Trump, J. R., Athanassoula, E., et al. 2015, MNRAS, 447, 506
Cisternas, M., Gadotti, D. A., Knapen, J. H., et al. 2013, ApJ, 776, 50
Cisternas, M., Jahnke, K., Inskip, K. J., et al. 2011, ApJ, 726, 57
Cisternas, M., Sheth, K., Salvato, M., et al. 2015, ApJ, 802, 137
Courteau, S., de Jong, R. S., & Broeils, A. H. 1996, ApJL, 457, L73
Croton, D. J., Springel, V., White, S. D. M., et al. 2006, MNRAS, 365, 11
Daddi, E., Alexander, D. M., Dickinson, M., et al. 2007, ApJ, 670, 173
Delvecchio, I., Lutz, D., Berta, S., et al. 2015, MNRAS, 449, 373
Donley, J. L., Koekemoer, A. M., Brusa, M., et al. 2012, ApJ, 748, 142
Ellison, S. L., Nair, P., Patton, D. R., et al. 2011, MNRAS, 416, 2182
Eskridge, P. B., Frogel, J. A., Pogge, R. W., et al. 2000, AJ, 119, 536
Fanali, R., Dotti, M., Fiacconi, D., & Haardt, F. 2015, MNRAS, 454, 3641
Ferrarese, L., & Merritt, D. 2000, ApJL, 539, L9
Fiore, F., Grazian, A., Santini, P., et al. 2008, ApJ, 672, 94
Friedli, D., & Benz, W. 1993, A&A, 268, 65
Gabor, J. M., & Bournaud, F. 2013, MNRAS, 434, 606
Galloway, M. A., Willett, K. W., Fortson, L. F., et al. 2015, MNRAS, 448, 3442
Gebhardt, K., Richstone, D., Kormendy, J., et al. 2000, AJ, 119, 1157
Georgakakis, A., Aird, J., Buchner, J., et al. 2015, MNRAS, 453, 1946
Georgakakis, A., Nandra, K., Yan, R., et al. 2008, MNRAS, 385, 2049
Gilfanov, M. 2004, MNRAS, 349, 146
Glikman, E., Simmons, B., Mailly, M., et al. 2015, ApJ, 806, 218
Goulding, A. D., & Alexander, D. M. 2009, MNRAS, 398, 1165
Goulding, A. D., Alexander, D. M., Bauer, F. E., et al. 2012a, ApJ, 755, 5
Goulding, A. D., Alexander, D. M., Lehmer, B. D., & Mullaney, J. R. 2010, MNRAS, 406, 597
Goulding, A. D., Forman, W. R., Hickox, R. C., et al. 2012b, ApJS, 202, 6
Goulding, A. D., Forman, W. R., Hickox, R. C., et al. 2014, ApJ, 783, 40
Graham, A. W., & Li, I.-H. 2009, ApJ, 698, 812
Hasinger, G., Miyaji, T., & Schmidt, M. 2005, A&A, 441, 417
Hickox, R. C., Jones, C., Forman, W. R., et al. 2007, ApJ, 671, 1365
Hickox, R. C., Jones, C., Forman, W. R., et al. 2009, ApJ, 696, 891
Hickox, R. C., & Markevitch, M. 2006, ApJ, 645, 95
Hickox, R. C., & Markevitch, M. 2007, ApJ, 671, 1523
Hickox, R. C., Mullaney, J. R., Alexander, D. M., et al. 2014, ApJ, 782, 9
Ho, L. C., Filippenko, A. V., & Sargent, W. L. W. 1997, ApJ, 487, 591
Hong, J., Im, M., Kim, M., & Ho, L. C. 2015, ApJ, 804, 34
Hopkins, P. F., & Hernquist, L. 2006, ApJS, 166, 1
Hopkins, P. F., & Quataert, E. 2010, MNRAS, 407, 1529
Hopkins, P. F., Somerville, R. S., Hernquist, L., et al. 2006, ApJ, 652, 864
Jogee, S. 2006, in Physics of Active Galactic Nuclei at all Scales, ed. D. Alloin (Berlin: Springer), 143
Jones, M. L., Hickox, R. C., Black, C. S., et al. 2016, ApJ, 826, 12
Juneau, S., Dickinson, M., Bournaud, F., et al. 2013, ApJ, 764, 176
Kocevski, D. D., Faber, S. M., Mozena, M., et al. 2012, ApJ, 744, 148
Kormendy, J., & Kennicutt, R. C., Jr. 2004, ARA&A, 42, 603
Kroupa, P. 2001, MNRAS, 322, 231
Lagos, C. D. P., Padilla, N. D., Strauss, M. A., Cora, S. A., & Hao, L. 2011, MNRAS, 414, 2148
LaMassa, S. M., Heckman, T. M., Ptak, A., et al. 2011, ApJ, 729, 52
Laurikainen, E., Salo, H., & Buta, R. 2004, ApJ, 607, 103
Lehmer, B. D., Alexander, D. M., Bauer, F. E., et al. 2010, ApJ, 724, 559
Lehmer, B. D., Basu-Zych, A. R., Mineo, S., et al. 2016, ApJ, 825, 7
Lintott, C., Schawinski, K., Bamford, S., et al. 2011, MNRAS, 410, 166
Lintott, C. J., Schawinski, K., Slosar, A., et al. 2008, MNRAS, 389, 1179
Magorrian, J., Tremaine, S., Richstone, D., et al. 1998, AJ, 115, 2285
Marchesi, S., Civano, F., Salvato, M., et al. 2016, ApJ, 827, 150
McConnell, N. J., & Ma, C.-P. 2013, ApJ, 764, 184
Menéndez-Delmestre, K., Sheth, K., Schinnerer, E., Jarrett, T. H., & Scoville, N. Z. 2007, ApJ, 657, 790
Mortlock, D. J., Warren, S. J., Venemans, B. P., et al. 2011, Natur, 474, 616
Noguchi, M. 1987, MNRAS, 228, 635
Oh, S., Oh, K., & Yi, S. K. 2012, ApJS, 198, 4
Pereira-Santaella, M., Alonso-Herrero, A., Santos-Lleo, M., et al. 2011, A&A, 535, A93
Reines, A. E., & Volonteri, M. 2015, ApJ, 813, 82
Revnivtsev, M., Churazov, E., Sazonov, S., Forman, W., & Jones, C. 2007, A&A, 473, 783
Robichaud, F., Williamson, D., Martel, H., et al. 2017, MNRAS, 469, 3722
Rosario, D. J., Mozena, M., Wuyts, S., et al. 2013, ApJ, 763, 59
Sánchez-Janssen, R., & Gadotti, D. A. 2013, MNRAS, 432, 56
Schawinski, K., Simmons, B. D., Urry, C. M., Treister, E., & Glikman, E. 2012, MNRAS, 425, L61
Schawinski, K., Treister, E., Urry, C. M., et al. 2011, ApJL, 727, L31
Sellwood, J. A. 2014, RvMP, 86, 1
Sheth, K., Vogel, S. N., Regan, M. W., Thornley, M. D., & Teuben, P. J. 2005, ApJ, 632, 217
Shlosman, I., Begelman, M. C., & Frank, J. 1990, Natur, 345, 679
Shlosman, I., Frank, J., & Begelman, M. C. 1989, Natur, 338, 45
Shlosman, I., & Noguchi, M. 1993, ApJ, 414, 474
Silverman, J. D., Kampczyk, P., Jahnke, K., et al. 2011, ApJ, 743, 2
Simmons, B. D., Urry, C. M., Schawinski, K., Cardamone, C., & Glikman, E. 2012, ApJ, 761, 75
Thacker, R. J., MacMackin, C., Wurster, J., & Hobbs, A. 2014, MNRAS, 443, 1125
Treister, E., Schawinski, K., Urry, C. M., & Simmons, B. D. 2012, ApJL, 758, L39
Ueda, Y., Akiyama, M., Ohta, K., & Miyaji, T. 2003, ApJ, 598, 886
Vasudevan, R. V., & Fabian, A. C. 2009, MNRAS, 392, 1124
Vito, F., Gilli, R., Vignali, C., et al. 2014, MNRAS, 445, 3557
Vito, F., Gilli, R., Vignali, C., et al. 2016, MNRAS, 463, 348
Vito, F., Vignali, C., Gilli, R., et al. 2013, MNRAS, 428, 354
Wada, K., & Habe, A. 1995, MNRAS, 277, 433
Wang, J., Kauffmann, G., Overzier, R., et al. 2012, MNRAS, 423, 3486
Willett, K. W., Lintott, C. J., Bamford, S. P., et al. 2013, MNRAS, 435, 2835
Worsley, M. A., Fabian, A. C., Bauer, F. E., et al. 2005, MNRAS, 357, 1281
Xue, Y. Q., Luo, B., Brandt, W. N., et al. 2011, ApJS, 195, 10
Xiao, T., Barth, A. J., Greene, J. E., et al. 2011, ApJ, 739, 28